Tailoring the surface density of silicon nanocrystals embedded in SiOx single layers

S. Hernández, P. Miska, M. Grün, S. Estradé, F. Peiró et al.

Citation: J. Appl. Phys. **114**, 233101 (2013); doi: 10.1063/1.4847536
View online: http://dx.doi.org/10.1063/1.4847536
View Table of Contents: http://jap.aip.org/resource/1/JAPIAU/v114/i23
Published by the AIP Publishing LLC.

Additional information on J. Appl. Phys.

Journal Homepage: http://jap.aip.org/
Journal Information: http://jap.aip.org/about/about_the_journal
Top downloads: http://jap.aip.org/features/most_downloaded
Information for Authors: http://jap.aip.org/authors

JOURNAL OF APPLIED PHYSICS **114**, 233101 (2013)

Tailoring the surface density of silicon nanocrystals embedded in SiO_x single layers

S. Hernández,[1] P. Miska,[2] M. Grün,[2] S. Estradé,[1,3] F. Peiró,[1] B. Garrido,[1] M. Vergnat,[2] and P. Pellegrino[1]

[1]*Electronics Department, MIND–IN2UB, Universitat de Barcelona, Martí i Franquès 1, E–08028 Barcelona, Catalonia, Spain*
[2]*Institut Jean Lamour, Université de Lorraine, CNRS UMR 7198—Faculté des Sciences et Technologies, B.P. 70239, F-54506 Vandoeuvre-lès-Nancy, France*
[3]*TEM–MAT, CCiT–UB, Scientific and Technological Center—Universitat de Barcelona, Solé i Sabarís 1, E–08028 Barcelona, Catalonia, Spain*

(Received 18 September 2013; accepted 29 November 2013; published online 16 December 2013)

In this article, we explore the possibility of modifying the silicon nanocrystal areal density in SiO_x single layers, while keeping constant their size. For this purpose, a set of SiO_x monolayers with controlled thickness between two thick SiO_2 layers has been fabricated, for four different compositions ($x = 1$, 1.25, 1.5, or 1.75). The structural properties of the SiO_x single layers have been analyzed by transmission electron microscopy (TEM) in planar view geometry. Energy-filtered TEM images revealed an almost constant Si-cluster size and a slight increase in the cluster areal density as the silicon content increases in the layers, while high resolution TEM images show that the size of the Si crystalline precipitates largely decreases as the SiO_x stoichiometry approaches that of SiO_2. The crystalline fraction was evaluated by combining the results from both techniques, finding a crystallinity reduction from 75% to 40%, for $x = 1$ and 1.75, respectively. Complementary photoluminescence measurements corroborate the precipitation of Si-nanocrystals with excellent emission properties for layers with the largest amount of excess silicon. The integrated emission from the nanoaggregates perfectly scales with their crystalline state, with no detectable emission for crystalline fractions below 40%. The combination of the structural and luminescence observations suggests that small Si precipitates are submitted to a higher compressive local stress applied by the SiO_2 matrix that could inhibit the phase separation and, in turn, promotes the creation of nonradiative paths. © *2013 AIP Publishing LLC*.
[http://dx.doi.org/10.1063/1.4847536]

I. INTRODUCTION

In the last two decades, silicon nanocrystals (Si-NCs) have been investigated for their fundamental properties as well as for potential applications in fields of electronics and photonics.[1,2] Recently, it has been proposed to use them in solar cells for down-conversion, to generate multi-excitons or as a top absorber in multifunction solar systems.[3–7] Several different methods for fabricating Si-NCs, all compatible with the semiconductor industry standards, have been developed, such as ion implantation,[8] cosputtering,[9] or plasma enhanced or low pressure chemical vapor deposition (CVD).[10] Even so, all these techniques face difficulties in accurately controlling the Si-NCs size and density, leading to a certain degree of uncertainty in interpreting how the actual Si-NCs morphology affects their electronic properties.

Many efforts have been put so far to control the Si-NCs size, either by controlling the silicon concentration, the post-deposition thermal process[8–10] or limiting the thickness of SiO_x layers between SiO_2 stoichiometric barriers (as the one proposed by Zacharias *et al.*[11]). Nevertheless, only few works can be found in literature dedicated to control and analyze the Si-NC areal density in similar systems.[12] The approaches used are generally based on an estimation of the Si-NC volumetric density by transmission electron microscopy (TEM) in samples with either bulk silicon-rich oxide (SRO) systems or SRO/SiO_2 multilayered samples and, through it, the areal density with large uncertainty.[12] In addition, changes in the density of nucleation centers can lead to Si-precipitates with structural properties strongly dependent on their environment.[13]

In the present work, we analyze the role of the silicon excess in the formation of Si-NCs in a single SiO_x layer, focusing the study on the modification of the Si-NC areal density. We use a direct method based on energy filtered TEM analysis applied to a single Si-NC layer to quantitatively evaluate this property. Additional high resolution TEM images from the same areas have been acquired, in order to determine the crystalline size of the Si precipitates. Finally, the optical properties of the Si-NC were monitored by means of photoluminescence (PL) measurements at 77 K. A direct correlation between the structural and optical properties has been established, finding that PL intensity scales with the crystalline degree of the Si aggregates. These observations suggest that, for stoichiometries close to that of SiO_2, the inhibited crystallization is related to the higher compressive local stress, which strongly affects the radiative transitions.

II. EXPERIMENTAL

Two different sets of samples with variable silicon concentration of SiO_x were fabricated by evaporation on (100) silicon

 © 2013 AIP Publishing LLC

substrates at 100 °C: samples with a single $SiO_2/SiO_x/SiO_2$ structure and samples containing 20 bilayers of SiO_x/SiO_2. The stoichiometric SiO_2 layers were deposited by evaporating targets of pure SiO_2, whereas the sub-stoichiometric SiO_x ones were obtained by co-evaporating SiO and SiO_2 from a thermal source and an electron beam gun, respectively. The final composition was obtained using different evaporation rates. Taking account the reaction $SiO_x \rightarrow (1\text{–}x/2)\ Si + x/2\ SiO_2$, the resulting silicon excesses in the SiO_x layers were of 25, 16, 10, and 5 atomic % (at. %) that correspond to relative oxygen-to-silicon concentrations of $x = 1$, 1.25, 1.5, and 1.75, respectively. In all samples, the thickness of the SiO_x layers was kept constant at 3 nm, while the SiO_2 barrier layers were of 9 nm and 5 nm, for the case of $SiO_2/SiO_x/SiO_2$ single layers and SiO_x/SiO_2 multilayers, respectively. During the evaporation of either SiO_x or SiO_2, the rate was monitored by a quartz microbalance and maintained constant at 0.1 nm/s. After deposition, the samples were annealed at 1050 °C for 5 min under nitrogen atmosphere in a rapid thermal annealing system.

The precipitation process was monitored by Fourier transform infrared spectroscopy in 200-nm thick SiO_x samples annealed at different temperatures (not shown), by following the shift of the position of the Si–O–Si asymmetric stretching mode. We found an excellent phase separation for all the used compositions when the samples are annealed at temperatures above 900 °C: in all samples, the Si-O-Si stretching mode presents a position ($\omega \approx 1080\ cm^{-1}$) and a lineshape typical for pure SiO_2 treated at this temperature or higher.

Slices for transmission electron microscopy using $SiO_2/SiO_x/SiO_2$ single layers were fabricated by the purely mechanical tripod method, in order to minimize any influence by the preparation method on the structural properties of the system. In-plane high resolution TEM (HRTEM) and energy filtered TEM (EFTEM) measurements were performed both in the same areas using a JEOL 2010F TEM operating at 200 keV coupled with a Gatan image filter, with a resolution in energy of 0.8 eV. In the case of EFTEM measurements, the Si contrast was enhanced by energetically filtering the TEM image, choosing only the electrons with an energy loss within a window around the Si plasmon energy ($E_{Si} = 17$ eV). Consequently, valuable information about the size and density of the precipitated Si nanoclusters of the single SiO_x layers can be extracted directly from those images.

PL measurements were performed on both sets of samples at 77 K in a liquid-nitrogen-cooled optical cryostat. The samples were excited by using the 313-nm line of a mercury arc lamp with a power density of 5 mW/cm^2, low enough to neglect any local temperature effects. The spectra were acquired in the range of 500–1000 nm and analyzed by using a monochromator equipped with a 150 grooves/mm grating and by a high sensitive CCD detector cooled at 140 K.

III. RESULTS AND DISCUSSION

TEM analysis was performed in $SiO_2/SiO_x/SiO_2$ single layers observed in planar view geometry. We present in Fig. 1, the energy filtered and high resolution TEM images of the precipitated Si-clusters in $SiO_2/SiO_x/SiO_2$ samples for different stoichiometries: $x = 1$, 1.25, 1.5, and 1.75. In the case of EFTEM images [Figs. 1(a)–1(d)], the bright spots correspond to silicon precipitates, while the darker grey areas correspond to SiO_2 (and the black region corresponds to the empty space beyond the sample). On the other hand, HRTEM images of the same areas are shown in Figs. 1(e)–1(h), where silicon crystallographic planes can be observed and distributed along the samples (see encircled areas). It is apparent in all the images that Si nanoaggregates have precipitated after the high

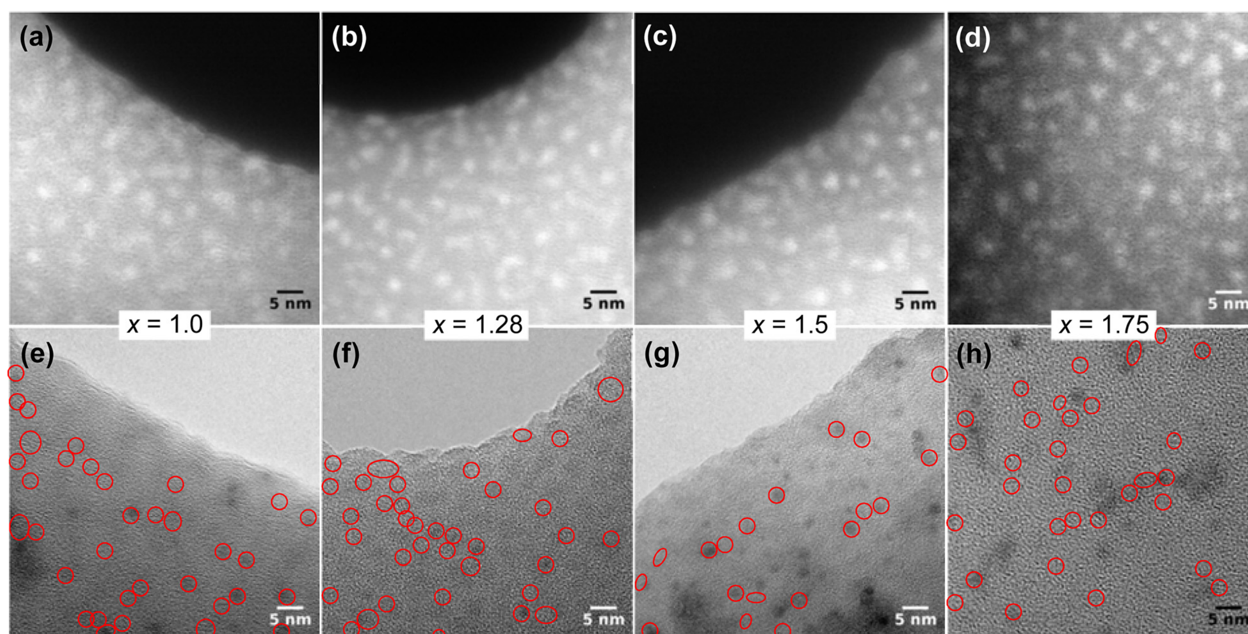

FIG. 1. Transmission electron microscopy images of $SiO_2/SiO_x/SiO_2$ single layers for different silicon stoichiometries: $x = 1$, 1.25, 1.5, and 1.75. Images from (a) to (d) were acquired by energy filtering the energy loss spectra around the Si-plasmon energy, while images from (e) to (h) were obtained using high resolution TEM (the crystalline clusters seen in the images are encircled in red). EFTEM and HRTEM images of each sample were taken in the same region.

temperature annealing for all the spanned range of stoichiometries, obtaining similar sizes and surface densities. For each sample, large areas have been analyzed to accurately determine both parameters. Consequently, size distribution of the whole cluster and their areal density can be extracted from EFTEM images, while the size distribution of the crystalline precipitates is obtained by means of HRTEM imaging (only the precipitates oriented along a high symmetry crystalline direction are observed using this configuration). Assuming that the Si-nanoaggregates have a spherical shape and are formed by a crystalline core surrounded by an amorphous shell (core-shell model[14,15]), EFTEM and HRTEM configurations are complementary, providing information either from the whole clusters or only on their crystalline core, respectively.

We found that the diameter of the Si-aggregates obtained by both configurations nicely follow a log-normal distribution, $f(d^{\mathrm{clu,cry}}, \sigma_{\mathrm{clu,cry}})$

$$f\left(d^{\mathrm{clu,cry}}, \sigma_{\mathrm{clu,cry}}\right) \propto e^{-\left[\frac{(\ln d_0^{\mathrm{clu,cry}} - \ln d^{\mathrm{clu,cry}})^2}{2\sigma^2_{\mathrm{clu,cry}}}\right]},$$

where $d^{\mathrm{clu,cry}}$, $d_0^{\mathrm{clu,cry}}$, and $\sigma_{\mathrm{clu,cry}}$ are the diameter, mean diameter, and broadening of the size distribution, respectively, for either whole clusters (clu) or crystalline cores (cry). Those parameters have been determined in all the samples by fitting the experimental distribution to the previous equation. In addition, the Si-NC areal density has been also determined using the data from EFTEM images. In Table I, we have summarized the results obtained from both techniques.

We have found that the diameter distribution of the whole cluster presents a similar distribution for all compositions, with a mean size d_0^{clu} around 2.7–2.8 nm (see Table I). The small discrepancies from sample to sample in the size distribution are the consequence of the uncertainty in the size determination, indicating that an almost identical size distribution is obtained for all stoichiometries. Nevertheless, the amount of Si-nanoaggregates is modified for the different samples, finding a variation of their areal density from $3.0 \times 10^{12}\,\mathrm{cm}^{-2}$ to $3.8 \times 10^{12}\,\mathrm{cm}^{-2}$, as the stoichiometry changes from $x = 1.75$ to $x = 1.0$. By using these values of areal density and mean sizes, the average distance between clusters was also evaluated. Even though the areal density variation is rather small, only around 30%, it is large enough to produce an important modification in the inter-dot distance. In fact, aggregates are separated by 2.2–2.4 nm for the highest silicon content (i.e., $x = 1.0$ and 1.25), while the average separation is much larger, taking values of 2.7 and 3.0 nm, for the lower silicon content ($x = 1.5$ and 1.75, respectively). This difference in the inter-dot distance can be directly observed on the EFTEM measurements: Si-NCs are very close to the adjacent ones in the samples with highest Si content [Figs. 1(a) and 1(b)], and are well separated in the samples with the lowest Si content [Figs. 1(c) and 1(d)].

Therefore, we demonstrated that, by employing $SiO_2/SiO_x/SiO_2$ structure-like systems and controlling the thickness and stoichiometry of the SiO_x layer, it is possible to modify the surface density, while keeping almost constant the size of Si precipitates.

Further analyses have been performed on the same set of samples (also on the same areas) by considering the images obtained by HRTEM [see Figs. 1(e)–1(h)]. We found that the mean crystalline diameter d_0^{cry} for each sample varies from 2.5 nm to 1.9 nm as the silicon content decreases (x from 1 to 1.75), values much smaller than the ones observed by EFTEM. As we mentioned above, this discrepancy is explained in terms of the amorphous Si-shell that surrounds the crystalline core.[14,15] We found that the thickness of the amorphous shell gets larger as the stoichiometry approaches the one of pure SiO_2, while the total cluster size is almost constant in all the explored range. The crystalline fraction (i.e., relative volume ratio between the crystalline and amorphous silicon regions) has been estimated by considering the size distribution of the whole clusters and the crystalline parts, obtained from the images of both TEM configurations. We observed that the crystalline fraction scales with the silicon content, with values ranging from 40% to 75% (see last column of Table I). Therefore, the stoichiometry of the SiO_x layers is affecting both the crystallinity and the areal density, obtaining a reduction of both magnitudes as the Si content is reduced.

The optical properties of the precipitated Si-nanoaggregates have been studied by means of PL. In Fig. 2(a), we present the PL emission of $SiO_2/SiO_x/SiO_2$ samples at 77 K, where a strong emission between 700 and 800 nm (typical from silicon nanoaggregates)[16,17] is observed only for samples with the highest silicon content (i.e., $x = 1.0$ and 1.25). The PL peak position of samples with $x = 1.0$ and 1.25 shifts to longer wavelengths, from 1.76 to 1.65 eV, respectively, as the silicon content decreases. Nevertheless, an intensity drop occurs as the silicon stoichiometry gets closer to SiO_2, getting no signal for samples with the lowest silicon content; i.e., $x = 1.5$ and 1.75. In fact, these samples with the lowest Si content present only a broad and weak defect-related emission in the blue-green region that is

TABLE I. Size distribution from the whole Si-cluster and from the crystalline core determined by EFTEM and HRTEM, respectively. The surface density was determined directly from the EFTEM images. The crystalline fraction has been calculated considering the size distribution obtained from both techniques.

	EFTEM			HRTEM		
x in SiO_x	Mean cluster diameter (nm), d_0^{clu}	Standard deviation (nm), σ_{clu}	Areal density ($\times 10^{12}\,\mathrm{cm}^{-2}$)	Mean crystalline diameter (nm), d_0^{cry}	Standard deviation (nm), σ_{cry}	Crystalline fraction, f_c
1.0	2.8	0.12	3.8	2.5	0.19	0.75
1.25	2.7	0.14	3.8	2.3	0.19	0.65
1.5	2.8	0.15	3.4	2.1	0.20	0.50
1.75	2.7	0.16	3.0	1.9	0.20	0.40

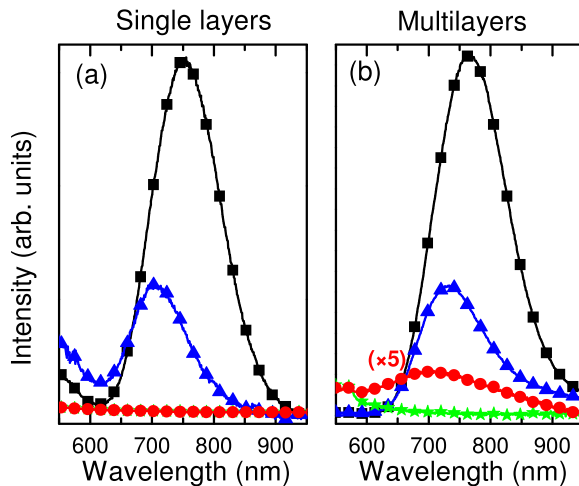

FIG. 2. PL spectra at 77 K of $SiO_2/SiO_x/SiO_2$ (a) single layers and (b) multilayered systems for samples with different silicon excesses. The square-line, triangle-line, circle-line, and star-line curves correspond to $x=1$, 1.25, 1.5, and 1.75, respectively.

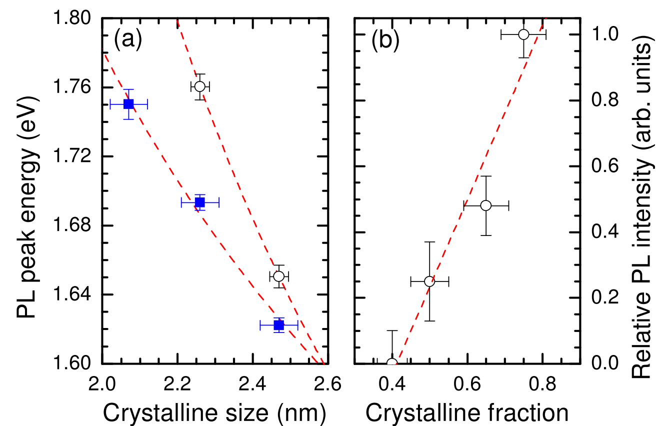

FIG. 3. (a) PL peak position of the $SiO_2/SiO_x/SiO_2$ single layers (open circles) and multilayered samples (full squares) for samples with different silicon excesses as a function of the crystalline size determined by HRTEM. (b) Relative PL intensity for the multilayered samples as a function of the crystalline fraction, normalized by the amount of Si atoms in crystalline state. The red-dotted lines are the best fits to (a) $E - E_{Si} = A/d^{\delta}$ equation or to (b) a linear trend.

associated to oxygen vacancy defects characteristics to amorphous SiO_x.[18]

In order to extract information of the optical emission from stoichiometries closer to SiO_2, special multilayered samples containing 20 periods of SiO_2/SiO_x bilayers nominally identical to the single layers were fabricated to increase their active volume and, in turn, their optical emission. In Fig. 2(b), we present the PL spectra of the multilayered samples for different stoichiometries. An intensity increase with respect to the single layers was observed in all the multilayered samples, which scales with the number of multilayers, allowing to detect Si-NC related emission also from sample $x=1.5$. Despite the fabrication of this new set of samples, no signal was observed for the lowest silicon content, $x=1.75$, which is a strong indication that sufficient crystallization is not yet attained for this composition, in agreement with our TEM observations.

The PL peak position in the multilayered samples presents the same trend than in the single SiO_x layers: there is a shift to shorter wavelengths as the silicon content decreases. However, there is a clear difference in the emission energy for single and multilayered samples with the same nominal stoichiometry: lower energy emission is observed for multilayered samples, compared to the single ones, of about 67 and 28 meV for $x=1$ and 1.5, respectively. In any case, the energy emission of both sets of samples lays well within the reported values found in the literature for samples with similar stoichiometry.[16,17]

Actually, the PL energy shift to higher energies observed in both sets of samples (single and multilayered ones) as the stoichiometry approaches to SiO_2 is related to an increase of electronic quantum confinement in small Si-NCs, favored by the low Si excess (the control of the Si content has been widely employed by many authors to tune their emission energy; see, for instance, Refs. 19 and 20). Therefore, the PL energy should be correlated to the size of the Si-aggregates. Through TEM characterization, we found that there is a similar Si-cluster size for all samples, but presenting a crystalline size reduction for lower Si content, in agreement with the PL energy band displacement for different stoichiometries. Consequently, we represented, in Fig. 3(a), the PL peak energy of the two sets of samples (single layers and multilayered samples) as a function of the crystalline size. For both sets of samples, the PL peak energy decreases for larger crystalline sizes following an inverse power law: $E - E_{Si} = A/d^{\delta}$,[21] being E_{Si} the band-gap energy of bulk silicon, d the crystalline diameter, and δ the decay factor. The obtained decay factor for multilayered samples was found to be 1.27, in very good agreement to report values in Si-NC embedded in SiO_2.[14,21] On the other hand, a larger δ was found for single layer samples, obtaining a value around 2.1. However, in the latter case only two points have been used for its determination, giving rise to a large inaccuracy. Nevertheless, the higher emission energy for the two sizes is a clear indication that a much larger δ value is associated to single layer samples.

Assuming that there is no change in the morphology of the precipitated Si-nanoaggregates in both sets of samples (the relative PL intensity between the two sets perfectly scales with the number of multilayers), the energy difference of some tenths of meV observed between single layer and multilayered samples could be related to a small loss of electronic confinement by interaction between adjacent SiO_x layers. Actually, the distance between adjacent layers in the multilayered samples is short enough (the SiO_2 barrier thickness is 5 nm) that can induce the excitonic migration between clusters, either via tunneling of individual electrons or holes, or by resonance energy transfers by a dipole-dipole coupling.[22] Both effects favorize the overlapping of the wavefunctions from Si-NCs in adjacent SiO_x layers, reducing the electronic quantum confinement. Consequently, the PL emission from Si-NCs in multilayered samples would present a peak energy slightly lower than the ones in single layer samples, as the latter ones are close to an isolated system. This effect is well established for CdSe nanocrystals[23] and has been previously observed in $Si\text{-}NCs/SiO_2$ systems,

presenting a slightly reduction in the electronic confinement energy as Si-NCs get closer.[24]

Another possible explanation arises by considering the different geometry of the two sets of samples (single or multilayers): thicker samples may be affected by a higher matrix induced compressive stress.[17,24,25] The total SiO_2 thickness is of 105 nm for the multilayered samples and only of 18 nm in the case of the single layer samples, exhibiting a difference of more than a factor 5. So, Si-NCs in multilayered samples are more influenced by the SiO_2 matrix and are also submitted to a higher compressive stress than in single layers. Recently, Kůsová *et al*. have reported the influence of the compressive stress in Si-NC/SiO_2 systems on the PL peak emission.[17] They conclude that there is a large red shift in PL when the Si-NCs are submitted to a high compressive stress, which is typically induced by the surrounding SiO_2 matrix. The PL emission from our two sets of samples lays in the scattered data corresponding to compressed Si-NC in Ref. 17, which suggests that single layers are also subjected to a strong influence from the SiO_2 environment. Nevertheless, it is needed to also consider that, apart from the SiO_2 from the above and below layers, the SiO_2 between Si-NCs in the same suboxide layer may also contribute to the stress over the nanostructures. From the structural characterization, we observed that the inter-dot distance increases for lower Si content (due to the reduction of their areal density), increasing as well the amount of SiO_2 surrounding the nanoaggregates. Consequently, the Si-NCs from SiO_x layers with lower Si content (i.e., smaller Si-NCs and larger inter-dot distance) are more likely to be submitted to a higher compressive stress than the ones from SiO_x layers with higher Si content (i.e., bigger Si-NCs and lower inter-dot distance), affecting also their emission properties.

Once the possible origins of the different emission energies of the two sets of samples have been evaluated, we have analyzed the intensity emission as the stoichiometry of the SiO_x layers is changed from $x = 1$ to $x = 1.75$. The multilayered samples were chosen for this comparison, as they present stronger emission than the single layers. As we commented above, there is a progressive intensity reduction of the PL integrated intensity as the stoichiometry approaches the one of SiO_2, scaling with the crystalline fraction. In Fig. 3(b), we have depicted the relative PL intensity evolution as a function of the crystalline fraction, once normalized to the amount of Si atoms in the crystalline state (considering their areal density and mean crystalline size from Table I). With a good approximation, we observe that the intensity linearly depends on the crystalline fraction, presenting no detectable emission for crystalline fraction below 40%. Therefore, there is an onset of PL emission of about $f_c \approx 40\%$, indicating that the crystalline fraction is playing a major role in reducing nonradiative paths, and thus, enhancing the PL intensity. Similar results were reported for partially crystalline Si-nanoclusters, observing PL only from nanoaggregates with a sizeable crystalline component and no emission from those with large amorphous component.[26]

The oxygen out-diffusion has been proved to be the mechanism involved in the local phase separation that allows Si crystallization.[13] Both structural and optical data point to an enhanced retardation of this diffusion for reduced Si excess, where the crystalline core of the precipitates is submitted to larger compressive stress. Higher annealing temperatures during longer times may produce Si-NCs with bigger crystalline domains, red-shifting and enhancing the PL emission and, at the same time, reducing the Si-amorphous phase. However, the use of large thermal budgets may induce the destruction of the multilayered/single layer structure, leading to a loss of control in the Si-NC size, density, and crystalline fraction.

IV. CONCLUSIONS

We analyzed the formation of silicon nanocrystals in single SiO_x layers with different stoichiometries, in order to explore the possibility of controlling the silicon nanostructure areal density. Using EFTEM and HRTEM, we have determined the size distribution of clusters and crystalline nanoaggregates. The size of the Si-clusters was found to be almost constant as the silicon content increases in the layers, whereas the areal density is slightly larger. The crystalline fraction of the nanoaggregates for each stoichiometry has been determined by combining the data from both TEM modes. The PL measurements show emission energies that increase as the stoichiometry gets closer to SiO_2, together with an intensity reduction. These observations are in good agreement with the TEM data, which indicate a reduction of the crystalline sizes and a loss of the crystalline fraction for lower Si excesses. Moreover, the PL emission linearly scales with the crystalline fraction, finding an onset of the PL emission for 40% crystalline fraction. In the layers with a low Si excess the weak PL emission, together with the reduced crystalline fraction, indicate that the phase separation is not sufficiently attainted for the outer suboxide shell of the small nanoaggregates that could have its origin in the high compressive local stress.

ACKNOWLEDGMENTS

The research leading to these results has received funding from the European Community's Seventh Framework Programme (FP7/2007-2013) under Grant Agreement No. 245977, under the project title NASCEnT. The present work was supported by the Spanish national project LEOMIS (TEC2012-38540-C02-01).

[1]L. Pavesi, L. D. Negro, C. Mazzoleni, G. Franzo, and F. Priolo, Nature **408**, 440 (2000).
[2]G. Franzò, A. Irrera, E. C. Moreira, M. Miritello, F. Iacona, D. Sanfilippo, G. Di Stefano, P. G. Fallica, and F. Priolo, Appl. Phys. A **74**, 1 (2002).
[3]W. D. A. M. de Boer, M. T. Trinh, D. Timmerman, J. M. Schins, L. D. A. Siebbeles, and T. Gregorkiewicz, Appl. Phys. Lett. **99**, 053126 (2011).
[4]M. C. Beard, K. P. Knutsen, P. Yu, J. M. Luther, Q. Song, W. K. Metzge, R. J. Elligson, and A. J. Nozik, Nano Lett. **7**, 2506 (2007).
[5]W. de Boer, H. Zhang, and T. Gregorkiewicz, Mater. Sci. Eng., B **159–160**, 190 (2009).
[6]D. Timmerman, J. Valenta, K. Dohnalova, W. D. A. M. de Boer, and T. Gregorkiewicz, Nat. Nanotechnol. **6**, 710 (2011).
[7]G. Conibeer, M. Green, R. Corkish, Y. Cho, E.-C. Cho, C.-W. Jiang, T. Fangsuwannarak, E. Pink, Y. Huang, T. Puzzer, T. Trupke, B. Richards, A. Shalav, and K. L. Lin, Thin Solid Films **511–512**, 654 (2006).

[8]M. L. Brongersma, A. Polman, K. S. Min, and H. A. Atwater, J. Appl. Phys. **86**, 759 (1999).
[9]S. Hayashi and K. Yamamoto, J. Lumin. **70**, 352 (1996).
[10]Y. Lebour, P. Pellegrino, S. Hernández, A. Martínez, E. Jordana, J. M. Fedeli, and B. Garrido, Physica E **41**, 990 (2009).
[11]M. Zacharias, J. Heitmann, R. Scholz, U. Kahler, M. Schmidt, and J. Blasing, Appl. Phys. Lett. **80**, 661 (2002).
[12]T. Z. Lu, M. Alexe, R. Scholz, V. Talalaev, R. J. Zhang, and M. Zacharias, J. Appl. Phys. **100**, 014310 (2006).
[13]M. Zacharias and P. Streitenberger, Phys. Rev. B **62**, 8391 (2000).
[14]F. Iacona, C. Bongiorno, C. Spinella, S. Boninelli, and F. Priolo, J. Appl. Phys. **95**, 3723 (2004).
[15]S. Hernández, A. Martínez, P. Pellegrino, Y. Lebour, B. Garrido, E. Jordana, and J. M. Fedeli, J. Appl. Phys. **104**, 044304 (2008).
[16]P. Miska, M. Dossot, T. D. Nguyen, M. Grün, H. Rinnert, M. Vergnat, and B. Humbert, J. Phys. Chem. C **114**, 17344 (2010).
[17]K. Kusová, L. Ondič, E. Klimešova, K. Herynková, I. Pelant, S. Daniš, J. Valenta, M. Gallart, M. Ziegler, B. Hönerlage, and P. Gilliot, Appl. Phys. Lett. **101**, 143101 (2012).
[18]D. Kovalev, H. Heckler, G. Polisski, and F. Koch, Phys. Status Solidi B **215**, 871 (1999).
[19]C. García, B. Garrido, P. Pellegrino, R. Ferré, J. A. Moreno, J. R. Morante, L. Pavesi, and M. Cazzanelli, Appl. Phys. Lett. **82**, 1595 (2003).
[20]B. Garrido, M. López, A. Pérez-Rodríguez, C. García, P. Pellegrino, R. Ferré, J. A. Moreno, J. R. Morante, C. Bonafos, M. Carrada, A. Claverie, J. de la Torre, and A. Souifi, Nucl. Instrum. Methods Phys. Res. B **216**, 213 (2004).
[21]M. I. Alonso, I. C. Marcus, M. Garriga, A. R. Goñi, J. Jedrzejewski, and I. Balberg, Phys. Rev. B **82**, 045302 (2010).
[22]V. A. Belyakov, V. A. Burdov, R. Lockwood, and A. Meldrum, Adv. Opt. Technol. **2008**, 1–32.
[23]C. B. Murray, C. R. Kagan, and M. G. Bawendi, Annu. Rev. Mater. Sci. **30**, 545 (2000).
[24]J. Linnros, N. Lalic, A. Galeckas, and V. Grivickas, J. Appl. Phys. **86**, 6128 (1999).
[25]J. S. Reparaz, A. Bernardi, A. R. Goñi, P. D. Lacharmoise, M. I. Alonso, M. Garriga, J. Novák, and I. Vávra, Appl. Phys. Lett. **91**, 081914 (2007).
[26]R. Anthony and U. Kortshagen, Phys. Rev. B **80**, 115407 (2009).